Supplementary Information

A microfluidic platform for systems pathology: multiparameter single-cell signaling measurements of clinical brain tumor specimens

Jing Sun[1-4,9], Michael Masterman-Smith[1-4,6,9], Nicholas A. Graham[1-4,9], Jing Jiao[1-4,9], Jack Mottahedeh[6], Dan R. Laks[6], Minori Ohashi[1-4], Jason DeJesus[5], Ken-ichiro Kamei[1-4], Ki-Bum Lee[1-4], Hao Wang[1-4], Zeta T.F. Yu[1-4], Yi-Tsung Lu[1,2], Shuang Hou[1-4], Keyu Li[1-4], Max Liu[1-4], Nangang Zhang[1,2], Shutao Wang[1-4], Brigitte Angenieux[6], Eduard Panosyan[6], Eric Samuels[1-4,6], Jun Park[1,2], Dirk Williams[1,2,4], Vera Konkankit[7], David Nathanson[2,5,8], R. Michael van Dam[1,2,4], Michael E. Phelps[1-4,8], Hong Wu[1-4,8], Linda M. Liau[7,8], Paul S. Mischel[2,3,5,8], Jorge A. Lazareff[7,8], Harley I. Kornblum[2,6,8], William H. Yong[5,8], Thomas G. Graeber[1-4,8,10], Hsian-Rong Tseng[1-4,8,10]

[1]Crump Institute for Molecular Imaging, [2]Department of Molecular and Medical Pharmacology, [3]Institute for Molecular Medicine, [4]California NanoSystems Institute, [5]Department of Pathology and Laboratory Medicine, [6]Department of Psychiatry, [7]Department of Neurosurgery, [8]Jonsson Comprehensive Cancer Center, University of California at Los Angeles, [9,10]These authors contributed equally to this work. Correspondence should be addressed to H.I.K (hkornblum@mednet.ucla.edu), W.H.Y. (wyong@mednet.ucla.edu), T.G.G. (tgraeber@mednet.ucla.edu) and H.R.T. (hrtseng@mednet.ucla.edu).

SUPPLEMENTAL METHODS

Fabrication of the cell array chips. The cell array chip consists of 24 (3 x 8) cell culture chambers, each with dimensions of 8 mm (l) x 1 mm (w) x 120 μm (h) for a total volume of 960 nL. The cell array chip is fabricated by directly attaching a polydimethylsiloxane (PDMS)-based microfluidic component onto a commercial poly-L-lysine (PLL)-coated glass slide (Polysciences, Inc., Philadelphia, PA) (Supplementary Fig. S1). The PDMS-based microfluidic component was fabricated using a soft lithography method. Well-mixed PDMS precursors (Sylgard 184, A:B = 10:1 ratio) were poured onto a silicon wafer replicate of photolithographically defined microchannel patterns. After vacuum degassing and curing at 80 ^{o}C, the microfluidic component was peeled off the replicate, followed by introduction of holes with pipette tip size-matched diameters at the ends of the microchannels. To attach the microfluidic component to a PLL-coated glass slide, we prepared a 1-3 μm-thick adhesive PDMS layer by spin coating a 1: 4 mixture of toluene and PDMS precursors (Sylgard 184, A:B = 5:1

ratio) onto a glass substrate. Through contact printing, the adhesive PDMS layer was directly transferred to the PDMS-based microfluidic component, followed by direct attachment onto a PLL-coated glass slide. The assembled chip was then baked in an 80 ^{o}C vacuum oven for 24 h. Prior to cell culture, the cell array chips were sterilized by exposure to UV light for 15 min. The cell suspension, culture media, and reagents were introduced into the cell array chips by an electronic, handheld pipette (Thermo Fisher Scientific, Hudson, New Hampshire).

Human tumor specimens. All patients were consented with approved UCLA Institutional Review Board protocols. Patient tumors were brought directly from neurosurgery suites of Ronald Reagan UCLA Medical Center upon resection and placed on ice for rapid portioning by the attending neuropathologist (WHY). Tumor portions were washed in PBS, minced with a scalpel blade and placed in TrypLE enzyme for 15 min at 37 ^{o}C. TrypLE supernatant was removed and replaced with DMEM-F12 (Gibco) and triturated with 3 successively smaller bore Pasteur pipettes (1). To remove cellular debris and red blood cells (RBCs) from tumor specimens, a Percoll purification procedure was used. First, we mixed Percoll (GE Healthcare) with a buffer (0.2 M Hepes, 0. 8 M NaCl and 1 M glycerol) at a 9:1 ratio and then mixed this Percoll solution with an equal volume of cells suspended in DMEM-F12. Second, the cell suspension was centrifuged at 1,000 g for 5 min. The pellet containing RBCs was discarded, and the supernatant was mixed with the Percoll buffer solution at a 1:2 ratio, followed by centrifugation at 3,000 g for 5 min. Third, the pellet containing cellular debris was discarded and the supernatant was diluted with DMEM-F12. Phenotypic comparison of Percoll-purified cell populations with unpurified specimens was made to verify that only RBCs and debris were removed during this process (MMS, JM, HIK, unpublished observations). Cells were filtered through a 40 μm single cell strainer (Becton Dickson) and loaded at a density of 50-250 cells/μL into PLL-coated chips and subjected to a centrifugation to facilitate cell attachment. Chips were then placed in a 10 cm petri dish with 1 mL ddH_2O to maintain humidity and

placed in 5% CO_2, 37 ^{o}C incubator for 15 min prior to on-chip ICC. Because immediate fixation of the tumor specimens prevented cell spreading, the tumor cells remained morphologically spherical in the MIC chip. To rule out potential artifacts associated with the tissue processing and on-chip MIC measurements, we verified that spherical U87 cells which had undergone an equivalent enzymatic digestion and MIC protocols exhibited no significant difference in the 4-parameter MIC data compared to the fully-spread U87 cells (Supplementary Fig. S14).

IHC Methods. IHC was carried out as previously described (2). Briefly, formalin-fixed, paraffin-embedded tissue samples were sectioned at 5 μm and mounted on slides which were then heated at 56 ^{o}C for 1 h, deparaffinized and hydrated. Endogenous peroxidase activity was blocked with 3% hydrogen peroxide before antigen retrieval was performed for 5 min at 120 °C in target retrieval solution (DAKO, Carpinteria, CA) in a pressure cooker. Sections were incubated with a monoclonal antibody against PTEN (clone 6H2.1, DAKO) at a dilution of 1:400. Antibody binding was detected using the Mach 4 Universal Polymer Detection System (Biocare Medical, Walnut Creek, CA) and visualized by Vector NovaRED substrate kit (Vector Laboratories, Burlingame, CA). Slides were counterstained with Mayers Hematoxylin. Individual slides were imaged at high magnification with an Aperio Slide Scanner (Vista, CA) and converted into TIFF files at a magnification of 10x. PTEN staining was analyzed and scored according to established methods (3).

On-chip Immunocytochemistry (ICC). On-chip ICC involved cell fixation (4% paraformaldehyde for 15 min at RT), washing with PBS, cell permeabilization (0.3% Triton X-100 for 15 minutes at RT), washing, blocking (10% normal goat serum, 3% BSA and 0.1% N-doceyl-B-maltodextrose for 12 h at 4°C), immunolabeling (12 h at 4°C) followed by washing and DAPI staining prior to microscopy-based image cytometry. During optimization of the MIC protocol, we tested several different methods for cell permeabilization (e.g., 0.1 %

Triton X-100 for 15 min, 0.3% Triton X-100 for 15 min, and ice-cold methanol for 20 min at -20 °C), and found that 0.3% Triton X-100 gave the largest difference between the positive and negative controls (e.g., U87-PTEN and U87 cells, respectively, for PTEN staining; see Fig. 2*A*), and thus chose this method for the MIC protocol. For immunolabeling, an optimized mixture of fluorophore-conjugated antibodies was prepared by mixing 2.754 μg/mL anti-EGFR (BD Pharmingen) labeled with LiCor/HiLyte Fluor 750 labeling kit (Dojindo Molecular Technologies, Inc.), 0.625 μg/mL PE-conjugated anti-PTEN (BD Biosciences), 1.250 μg/mL Alexa Fluor 647-conjugated anti-pS473-AKT (Cell Signaling Technology) and 3.800 μg/mL Alexa Fluor 488-conjugated antipS235/S236-S6 (Cell Signaling Technology). All liquid/buffer exchanges were done using a semi-automated micropipette that regulated pipetting speeds and thus protected the cells from shear forces.

Image Acquisition and Processing. The MIC chip containing immunostained cells was mounted onto a Nikon TE2000S inverted fluorescent microscope with a CCD camera (Photomatrix, Cascade II), X-Cite 120 Mercury lamp, automatic stage, and filters for five fluorescent channels (W1(DAPI), W2(Alexa Fluor 488), W3(PE), W4(Alexa Fluor 647) and W5(HiLyte Fluor 750)). A FocalCheck fluorescence microscope test slide from Invitrogen was used for light source emission calibration. For U87 cell lines, the exposure times are 10 sec for HiLyte Fluor 750 (EGFR), 0.1 sec for PE (PTEN), 2 sec for Alexa Fluor 647 (pAKT) and 0.2 sec for Alexa Fluor 488 (pS6). For tumor specimens, the exposure times were identical except 1 sec for PE and 0.5 sec for Alexa Fluor 488. After image acquisition, MetaMorph (Molecular Devices, Version 7.5.6.0) was used to quantify fluorescent signals in individual cells using the Multi-Wavelength Cell Scoring module. A nuclei counting application allowed exclusion of debris from analysis. Background subtraction for each frame was performed by assessing the average intensity values in area with no cells. Fluorescent intensity values were normalized by the cell-spread-surface-area and data were logarithmically transformed to create Gaussian-like distributions for subsequent analysis.

Rank-based analysis of MIC measurements. To emphasize the quantitative, single-cell nature of the MIC technology, we plotted clinical tumor specimen MIC measurements on rank-based graphs to demonstrate relative expression of EGFR, PTEN, pAkt and pS6. Briefly, cells from several tumor specimens that spanned a range of expression values were sorted from lowest to highest expression. This compendium of single-cell expression values was then segregated into different rows, with each row representing one tumor specimen. For each row, if a cell was originally found in the tumor specimen corresponding to that row, a single bar was placed to represent that cell. To represent the intensity of expression, each bar was shaded on a green to red color scale. For expression values not present in the row corresponding to a particular tumor specimen, those bars were colored gray.

Bioinformatic analysis of MIC data. Self-organizing maps (SOMs) were created in R using the *Kohonen* package of Wehrens & Buydens (4). Briefly, a SOM grid consists of a set of units which are each characterized by a codebook vector; here, each codebook vector consists of four values (EGFR, PTEN, pAkt and pS6). Before SOM training, the input MIC measurements were unit normalized. The codebook vectors are then randomly initialized based on the input data and subjected to a training process that involves repeated presentation of the training data to the map. Each presented piece of data is assigned to a "winning" (or most similar) grid, and the codebook vector of the winning grid is updated using a weighted average, where the weight is the learning rate α (here 0.05). Because each training process involves random initialization of the codebook vectors and thus distinct map topologies, three SOMs were trained for each data set, and the resulting maps were examined for qualitative consistency. Additionally, we tested various SOM grid sizes and found that 49 (7x7) hexagonally-packed units was the smallest size the captured the qualitative differences between tumor samples (Supplementary Figs. S11 and S12).

For SOM training, the input data set is a compendium of many measurements that represent the global measurement space. Here, the input training data set consisted of ~40,000 single-cell 4-parameter measurements from 19 tumor specimens (1,000-2,800 cells per sample). After training, the individual samples from the compendium were then be mapped to the SOM to indicate which portion of the parameter space is occupied by an individual sample. This mapping procedure involves assessment of the best-matching SOM unit for each single-cell 4-parameter measurement in the data set, followed by assignment of that single-cell measurement to the best-matching unit. Running R Version 2.8.1 on a desktop PC with a 2.66 GHz processor, SOM training and mapping of the patient sample data set required less than 1 minute of computational time. To normalize for different number of cells analyzed across data sets, we then convert the number of cells in each unit to a frequency. Thus, regions of a SOM mapping that have a large frequency of cells indicate that many cells within that data set closely resemble the 4-value codebook vector that characterizes that unit. To cluster the SOM mappings of the tumor specimens, we calculated a neighborhood frequency (the sum of the frequencies for a unit and its neighbors, Supplementary Fig. S12*A*). These values were then subjected to unsupervised hierarchical clustering using the average-linkage method based on the Pearson correlation using Cluster software (5). Data were visualized using Java Treeview (6).

Step-wise operational protocol.

Chip Fabrication

1. 40 g of polydimethylsiloxane (PDMS) precursors (Sylgard 184, A:B = 10:1 ratio) were mixed using a commercial mixer.
2. Aluminum foil was pressed into the internal surface of a 10 cm Petri dish to allow easy removal of PDMS mold and silicon wafer template.

3. A silicon wafer template with raised etching of photolithographically-defined microchannel patterns (of 4 individual cell array chips per template) was placed in the bottom of the dish.
4. PDMS contents (in liquid form) were poured over the silicon wafer.
5. A disposable syringe needle was gently applied to the silicon wafer to push air and PDMS out from under the wafer and push the wafer to the bottom of the Petri dish.
6. The dish was placed in a vacuum degasser for 1 h to remove all air bubbles from the liquid PDMS.
7. The dish was transferred to a 80 ^{o}C oven and cured for 2 h.
8. The solid PDMS mold was allowed to cool to room temperature.
9. Aluminum foil surrounding the silicon template and PDMS mold was gently removed from the Petri dish.
10. Aluminum foil and any excess PDMS in between the silicon template and the aluminum foil was cut away from the under-side of the template with a razor blade.
11. The PDMS mold was gently peeled away from the silicon template.
12. The 4 microfluidic cell array chips were cut out of the PDMS mold with a razor blade.
13. Each chip had holes introduced with pipette tip sized-matched diameters at the ends of the microchannels using a manual hole puncher.
14. A 1:4 mixture of toluene and PDMS precursors (Sylgard 184, A:B = 5:1 ratio) was hand-mixed for attachment of the PDMS microfluidic chip to a microscope slide.
15. The PDMS-toluene adhesive mixture was dripped onto a glass microscope slide and then spun at 4,000 RPM for 1 min to coat the slide with a 1-3 μm-thick layer of the adhesive mixture.
16. Each PDMS microfluidic chip was placed on the adhesive PDMS-toluene layer to coat the under-surface of the chip with adhesive.
17. Each PDMS microfluidic chip was then directly transferred onto a commercially available poly-L-

lysine (PLL)-coated glass slide (Poly Sciences) with gentle uniform pressure across the chip.

18. Each assembled microfluidic cell array chip was transferred to 80 ^{o}C vacuum oven and baked for 24 h.
19. Each assembled microfluidic cell array chip was placed in a Petri dish and sterilized by exposure to UV light for 15 min.

Tumor Collection and Dissociation into Single Cells

1. Upon tumor resection, tissue was placed on ice for rapid portioning by the attending neuropathologist (WY). Steps 2-5 occur within 30 min of tumor resection:
2. Tumor portions were washed in PBS, minced with a scalpel blade and placed in TrypLE enzyme for 15 min at 37 ^{o}C. TrypLE supernatant was removed and replaced with DMEM-F12 (Gibco) and triturated with 3 successively smaller bore Pasteur pipettes (1).
3. To remove cellular debris and red blood cells (RBCs) from tumor specimens, a Percoll purification procedure was used. First, we mixed Percoll (GE Healthcare) with a buffer (0.2 M Hepes, 0. 8 M NaCl and 1 M glycerol) at a 9:1 ratio and then mixed this Percoll solution with an equal volume of cells suspended in DMEM-F12. Second, the cell suspension was centrifuged at 1,000 g for 5 min. The pellet containing RBCs was discarded, and the supernatant was mixed with the Percoll buffer solution at a 1:2 ratio, followed by centrifugation at 3,000 g for 5 min. Third, the pellet containing cellular debris was discarded and the supernatant was diluted with DMEM-F12.
4. Cells were filtered through a 40 μm single cell strainer (Becton Dickson).
5. Cell densities are dependent on the size of original sample. A 100-500 μL aliquot of media containing single cells was spun down at 1,200 RPM for 1 min and then resuspended at a density of 50-500 cells/μL. A Matrix semi-automated pipettor (Thermo Fisher Scientific, Hudson, New Hampshire) fitted with 12.5 μL pipet tips was used to transfer suspended cells into PLL-coated microfluidic chips at a rate for 6.0 μl/sec.

6. After cell-loading, chips were centrifuged at 1,000 RPM for 1 min to facilitate cell attachment.
7. Chips were placed in a 10 cm petri dish with 1 mL ddH_2O (to maintain humidity) and placed in 5% CO_2, 37 ^oC incubator for 15 min.

'On-chip' Immunocytochemistry

For all immunocytochemistry steps, liquids are introduced to the chip using semi-automated pipetting at 0.55 µl/sec to reduce shear forces on cells.

1. Cells were fixed by loading 4 µL 4% paraformaldehyde and maintained for 15 min at room temperature.
2. Cells were washed 3 times with 4 µL PBS.
3. Cells were permeabilized with 0.3% Triton X-100 for 15 min at room temperature
4. Cells were washed 1 time with 4 µL PBS.
5. Cells were blocked with a mixture of 10% normal goat serum, 3% bovine serum albumin and 0.1% N-doceyl-B-maltodextrose and kept for 12 h at 4 °C.
6. Cells were immunolabeled with an optimized mixture of fluorophore-conjugated antibodies consisting of 2.754 µg/mL anti-EGFR (BD Pharmingen) labeled with LiCor/HiLyte Fluor 750 labeling kit (Dojindo Molecular Technologies, Inc., Rockville, MD), 0.625 µg/mL PE-conjugated anti-PTEN (BD Biosciences), 1.250 µg/mL Alexa Fluor 647-conjugated anti-pS473-AKT (Cell Signaling Technology) and 3.800 µg/mL Alexa Fluor 488-conjugated anti-pS235/S236-S6 (Cell Signaling Technology) and maintained at 4 °C for 12 h.
7. Cells were washed 1 time with 4 µL PBS. To prevent exposure of external chip surfaces to antibody, a 12 µL Matrix pipet tip was inserted at the effluent to recover antibody.
8. Cell nuclei were stained with DAPI for 5 min at room temperature.
9. Cells were washed 3 times with PBS.

Image acquisition

1. The chip containing immunostained cells was mounted onto a Nikon TE2000S inverted fluorescent microscope with a CCD camera. The size of each channel had a width designed for edges to be outside the imaging area. Each channel had a length permitting 8 imageable 'frames', and all frames were used for image analysis. Exposure times were 10 sec for HiLyte Fluor 750 (EGFR), 1 sec for PE (PTEN), 2 sec for Alexa Fluor 647 (pAKT) and 0.5 sec for Alexa Fluor 488 (pS6).
2. MetaMorph (Molecular Devices, Version 7.5.6.0) was used to quantify fluorescent signals in individual cells. The Multi-Wavelength Cell Scoring module allowed image analysis for expression intensity scoring and quantification of cells from the 4 fluorophore-labeled antibodies (W2-488nm, W3-PE, W4-647nm and W5-750nm). DAPI (W1) allowed nuclei counting to exclude debris from analysis. After setting minimum and maximum cell size thresholds, Metamorph identifies "cell regions," which were manually inspected by the user to verify that all cells (but not cell debris) were accurately identified by the Metamorph algorithm. Finally, the fluorescent intensity for each cell region was quantified.
3. Background subtraction for each frame was performed by assessing the average intensity values in areas with no cells and subtracting this intensity value from each cell's score for each fluorescent signal.
4. Integrated fluorescent intensity values were then divided by the cell area to achieve a cell-spread-surface-area average intensities, and these values were logarithmically transformed to give Gaussian-like distributions. Log-transformed values were used for subsequent analysis.

SOM Construction

1. Using R Version 2.8.1, the Kohonen package for creation and analysis of self-organizing maps was downloaded (http://cran.r-project.org/web/packages/kohonen/index.html), installed and loaded.
2. MIC measurements from each individual patient were aggregated into a global data set of ~40,000 4-parameter measurements and mean normalized.

3. Using the *som* command in R, a 7x7 hexagonally-packed SOM was trained using the mean-normalized data set with 100 iterations and a learning rate (α) of 0.05. Because each training process involves random initialization of the codebook vectors and thus distinct map topologies, three SOMs were trained for each data set, and the resulting maps were examined for qualitative consistency. Running R Version 2.8.1 on a desktop PC with a 2.66 GHz processor, SOM training and mapping of the patient sample data set required less than 1 minute of computational time.
4. The resulting SOMs were checked for a) convergence (as measured by the average distance of an object with the closest codebook vector unit) and b) quality (the mean similarity of objects mapped to a unit to the codebook vector of that unit).

Mapping of patient samples to the SOM

1. For a given SOM, the *map* command in R was used to map the MIC measurements for each individual patient to the SOM.
2. Using the *hist* command, the number of cells mapped to each SOM unit was calculated and then converted to a frequency.
3. The $\log_2$ frequencies were plotted on the SOM grid using a rainbow color scale.
4. This mapping process was repeated for each of the three trained SOMs, and individual patient sample mappings were examined for qualitative consistency.

Clustering of SOM mappings

1. For each patient sample mapping, the Neighborhood Frequency Vector was calculated (Supplementary Fig. S12*A*).
2. These NFVs were subjected to unsupervised hierarchical clustering using the average-linkage method based on the Pearson correlation using Cluster software (5).
3. Data were visualized using Java Treeview 1.1.3 (6).

SUPPLEMENTARY TABLES

Supplementary Table S1. Patient and tumor characteristics.

Pt ID	Age (years)	Cells Analyzed	Progression-free survival from resection (days)	Overall survival from resection (days)	Additional Treatment	Pathology	Grade	SOM Cluster	IHC PTEN % Cells Intact
1	47	1894	461	552	Carboplatin/Avastin/Proton Radiation	GBM	IV	I	40-70 %
2	66	1170	525	525	Temodar	GBM	IV	II	100%
3	7	2841	265	265	Temodar	Pilocytic Astrocytoma	I	I	Not Analyzed
4	84	1448	255 -	255 -	-	GBM	IV	III	40%
5	39	1903	430	430	Gamma Knife Radiosurgery	GBM	IV	I	10-20 %
6	44	2010	413	413	Temodar	Oligoastrocytoma	III	III	100%
7	39	1765	176	252	Gamma Knife Radiosurgery	GBM	IV	I	100%
8	32	2117	379	379	Radiotherapy	Anaplastic Oligoastrocytoma/No tumor	III	I	0%
9	50	2615	174 -	317 -	-	Gliosarcoma	IV	III	30-40 %
10	81	1940	166	411	Avastin	GBM	IV	III	0%
11	49	2166	334	334	-	Oligodendrioglioma	III	III	Not Analyzed
12	70	2264	72 -	72 -	Temodar/Enzastaurin	GBM	IV	II	100%
13	24	2318	326	326	-	Oligodendrioglioma	II	I	Not Analyzed
14	7	972	192 -	302 -	Radiotherapy	GBM	IV	II	100%
15	81	2136	100 -	100 -	-	GBM	IV	III	95%
16	62	2417	45 -	45 -	-	GBM	IV	II	10%
17	53	2384	354	361	Radiotherapy/Gliadel/Temodar	Gliosarcoma	IV	III	30-40 %
18	0.75	2508	(42)	(42)	-	Pilocytic Astrocytoma	I	I	Not Analyzed
19	4.75	2374	76	76	-	DNET	I	I	Not Analyzed

Demographic and pathologic description for the 19 patient samples examined in this study. Progression-free survival and Overall survival is shown from the date of tumor resection (i.e., when sample was obtained for MIC analysis). Pt ID = patient identification number, Cells Analyzed = number of cells measured by the MIC technology, # MIC Channels refers to the number of MIC channels that were loaded with cells. MIC measurements did not correlate with either the total number of cells measured or the number of cells per MIC channel (data not shown). Within the columns for Progression-free survival and Overall survival, "-"indicates deceased, and parentheses indicate that the patient was lost to follow-up. GBM = glioblastoma, DNET = Dysembryoplastic neuroepithelial tumor. Grading corresponds to WHO classification. Although PTEN scoring was available for patients 8, 9, 16 and 17, these samples were excluded from comparison to clinical IHC methods (Fig. 3*A*) due to differential diagnoses (Patients 8, 9 and 16) or therapeutically-induced changes in parts of the diagnostic tissue (Patient 17) data not shown).

SUPPLEMENTARY FIGURES

Supplementary Figure S1. Schematic representation of cell array chip fabrication.

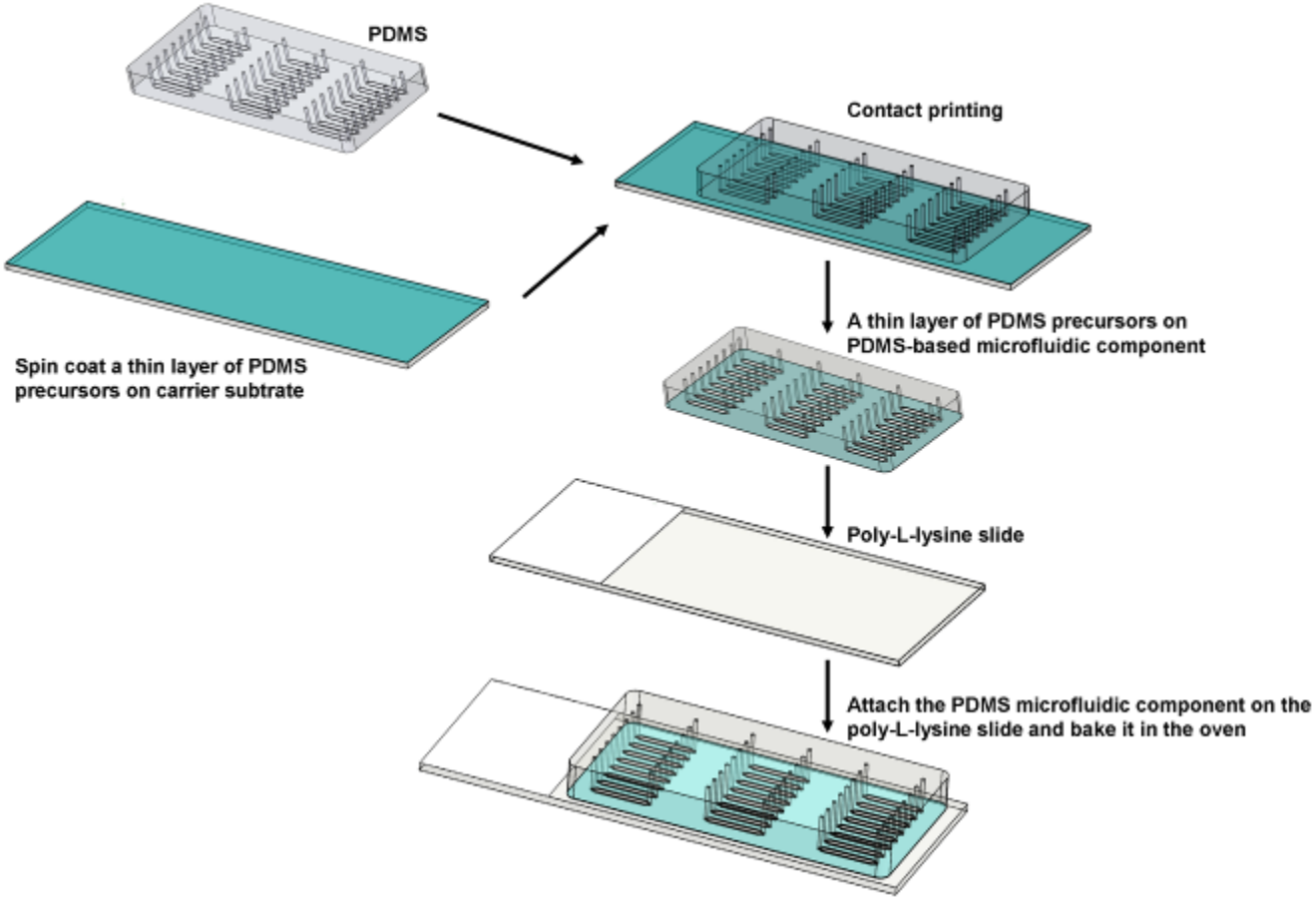

The cell array chip is fabricated by directly attaching a polydimethylsiloxane (PDMS)-based microfluidic component onto a commercial poly-L-lysine (PLL)-coated glass slide. The PDMS-based microfluidic component was fabricated using soft lithography methods. Well-mixed PDMS precursors were poured onto a silicon wafer replicate of photolithographically defined microchannel patterns. To attach the microfluidic component to the PLL-coated glass slide, we prepared a 1-3 μm thick adhesive PDMS layer by spin coating a mixture of toluene and PDMS precursors onto a glass substrate. Through contact printing, the adhesive PDMS layer was directly transferred to the PDMS-based microfluidic component, followed by direct attachment to a PLL-coated glass slide. The assembled chip was then baked in an 80 °C vacuum oven for 24 hours.

Supplementary Figure S2. Cell/fluid/reagent delivery for the MIC.

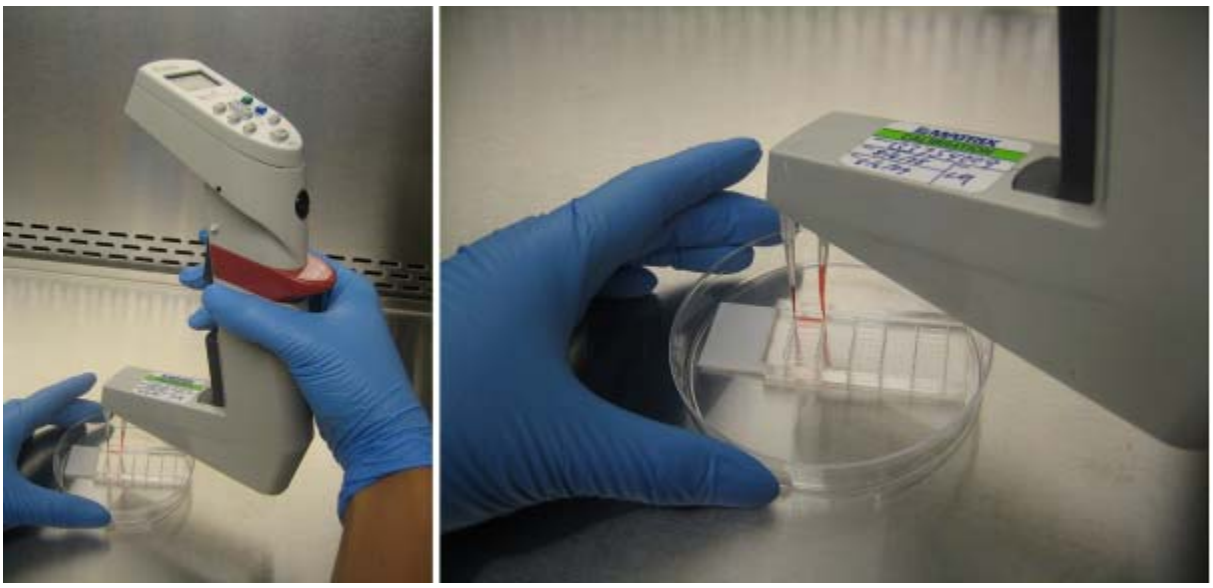

Precise delivery of cells, fluids and reagents to the MIC cell culture chambers is achieved by using a digitally-controllable Matrix™ pipettor with a 12.5 µL pipette tips aligned with the chamber inlet. To serve as a reservoir for the waste solution, a second pipette tip is placed in the chamber outlet.

Supplementary Figure S3. Growth curve for U87 isogenic cell lines cultured on-chip.

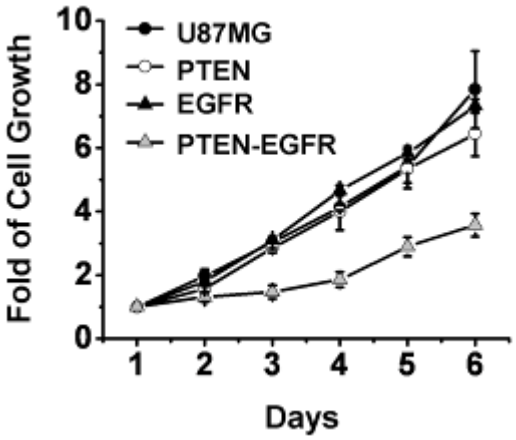

Each U87 isogenic cell line (U87, U87-PTEN, U87-EGFR and U87-PTEN-EGFR) was loaded into four chambers of the MIC chip at a concentration of 200-400 cells per chamber. For six days, cell growth was monitored by collecting bright field micrographs of cells (8 fields/channel) inside the chip, and data were normalized to Day 1. By comparing to previously published data (7), we confirmed that the microfluidic environment did not affect proliferation rates compared to off-chip culture conditions.

Supplementary Figure S4. MIC measurements of PTEN exhibit minimal cross reactivity with other fluorophore-labeled monoclonal antibodies (i.e., anti-EGFR, anti-pAkt and anti-pS6).

A)

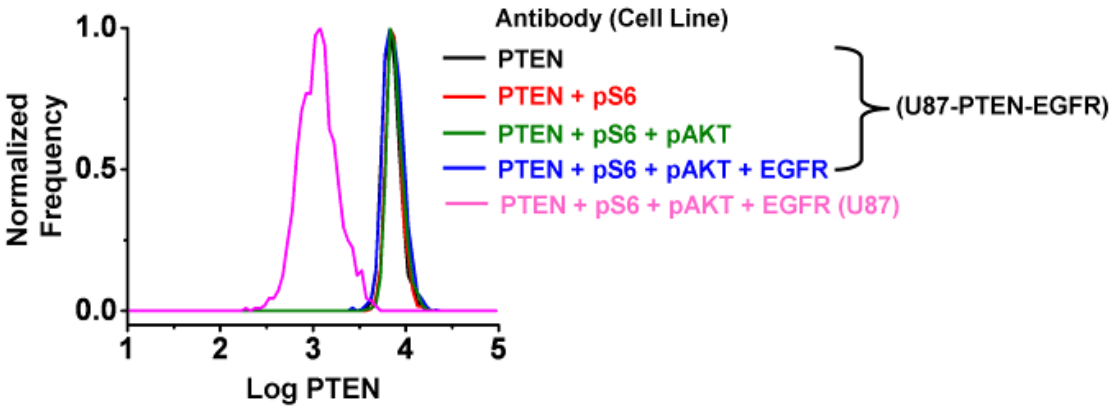

B)

	Reproducibility of PTEN quantification in the presence of other antibodies			
Stain(s) included	PTEN	PTEN & pS6	PTEN, pS6 & pAkt	PTEN, pS6, pAkt & EGFR
Mean	3.84	3.87	3.87	3.88
Mean Shift (raw units)		-0.026	0.004	-0.018
Mean Shift (%)		-0.67%	0.11%	-0.47%
	Compared to staining of PTEN without other antibodies			
t-score	-	-0.21	-0.15	-0.31
p -value	-	0.16	0.12	0.24

C)

	PTEN quantification compared to the negative control cell line U87			
Stain(s) included	PTEN	PTEN & pS6	PTEN, pS6 & pAkt	PTEN, pS6, pAkt & EGFR
t-score	3.45	3.63	3.45	3.66
p -value	2.9E-04	1.5E-04	2.9E-04	1.3E-04

To test the cross reactivity among the four fluorophore-labeled monoclonal antibodies (LiCor/ HiLyte Fluor 750-labeled anti-EGFR, PE-conjugated anti-PTEN, Alexa Fluor 647-conjugated anti-pAKT and Alexa Fluor 488-conjugated anti-pS6) used in the optimized ICC protocol, we quantified PTEN expression in U87-PTEN cells after staining with PTEN antibody alone (PTEN), a cocktail of two antibodies (PTEN & pS6), a cocktail of three antibodies (PTEN, pS6 & pAkt) and the cocktail of four antibodies (PTEN, pS6, pAkt & EGFR). For

each antibody cocktail, the concentrations of the monoclonal antibodies were kept identical in all experiments. *A*, Histograms of PTEN expression demonstrate minimal cross reactivity in the presence of other fluorophore-labeled antibodies. For reference, we have included the histogram of PTEN measurements from the negative control (U87 cells stained with the cocktail of four antibodies). *B*, Statistical analysis of cross-reactivity among fluorophores. To confirm that the histograms of PTEN were not significantly shifted in the presence of the other fluorophore-labeled antibodies, we calculated the t-score ($[\mu_{\text{sample 1}} - \mu_{\text{sample 2}}] / [(\sigma_{\text{sample 1}})^2 + (\sigma_{\text{sample 2}})^2]^{½}$ where μ is the sample mean and σ is the sample standard deviation) between cells stained for PTEN alone and those stained with antibody cocktails. All log-transformed data were approximately normally distributed. All the calculated *p*-values were all less than 0.25, suggesting that the mean signal was highly similar across all samples, even in the presence of other fluorophore-labeled antibodies. *C*, Statistical analysis of reproducibility of PTEN measurements versus negative controls. To confirm that PTEN measurements were reproducibly different compared to the negative control cell line U87, we calculated the t-score for the PTEN histogram from each antibody cocktail and found very small *p*-values ($p < 0.001$), indicating that these antibody cocktails did not affect the performance of the MIC technology.

Supplementary Fig. S5. Statistical analysis of the reproducibility of MIC measurements.

A)

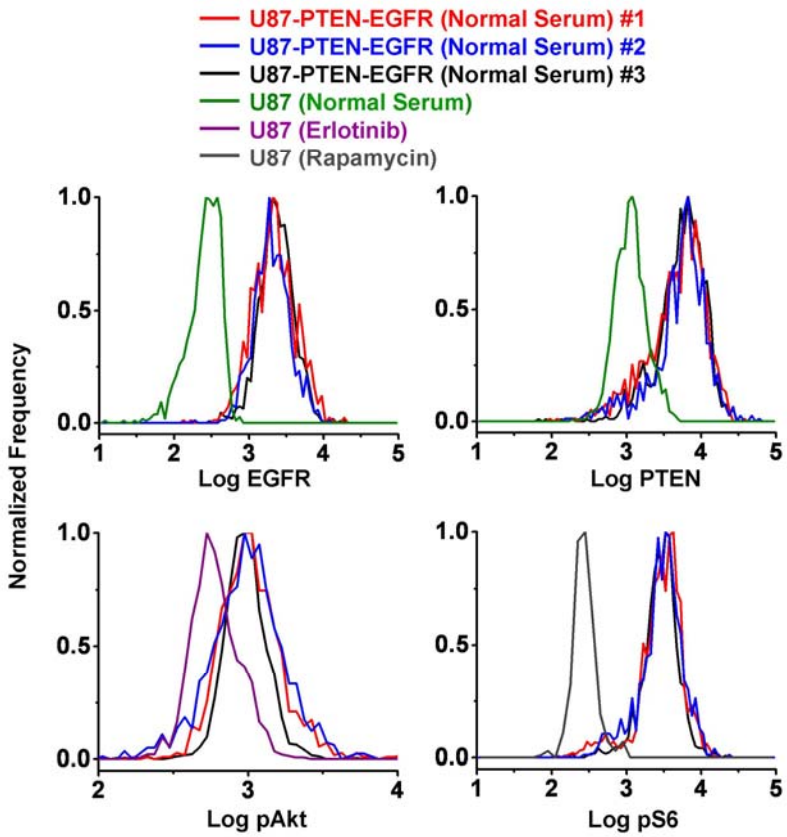

B)

Reproducibility among replicate measurements of EGFR, PTEN, pAkt and pS6

EGFR			
Replicate	#1	#2	#3
Mean	3.37	3.34	3.31
Mean Shift (raw units)		0.034	0.029
Mean Shift (%)		1.0%	0.9%

EGFR			
Comparison	#1 vs. #2	#1 vs. #3	#2 vs. #3
t-score	0.09	0.19	0.08
***p* -value**	0.07	0.15	0.06

PTEN			
Replicate	#1	#2	#3
Mean	3.73	3.66	3.70
Mean Shift (raw units)		0.072	-0.044
Mean Shift (%)		2.1%	-1.3%

PTEN			
Comparison	#1 vs. #2	#1 vs. #3	#2 vs. #3
t-score	0.14	0.05	0.08
***p* -value**	0.11	0.04	0.06

pAkt			
Replicate	#1	#2	#3
Mean	2.98	3.03	3.38
Mean Shift (raw units)		-0.050	-0.350
Mean Shift (%)		-1.7%	-11.7%

pAkt			
Comparison	#1 vs. #2	#1 vs. #3	#2 vs. #3
t-score	0.17	1.38	0.98
***p* -value**	0.14	0.83	0.67

pS6			
Replicate	#1	#2	#3
Mean	3.45	3.25	3.46
Mean Shift (raw units)		0.207	-0.216
Mean Shift (%)		6.9%	-7.2%

pS6			
Comparison	#1 vs. #2	#1 vs. #3	#2 vs. #3
t-score	0.41	0.02	0.41
***p* -value**	0.32	0.02	0.31

C)

Reproducibility of replicate measurements versus negative controls

	EGFR staining compared to U87			PTEN staining compared to U87		
	Replicate #1	Replicate #2	Replicate #3	Replicate #1	Replicate #2	Replicate #3
t-score	2.95	2.56	2.73	1.77	1.34	1.50
***p*-value**	3.2E-03	1.1E-02	6.5E-03	0.08	0.18	0.13

	pAkt staining compared to U87-PTEN-EGFR + erlotinib			pS6 staining compared to U87-PTEN-EGFR + rapamycin		
	Replicate #1	Replicate #2	Replicate #3	Replicate #1	Replicate #2	Replicate #3
t-score	0.94	0.84	2.01	3.54	1.73	3.08
***p*-value**	0.35	0.40	0.04	4.2E-04	8.5E-02	2.1E-03

To test the reproducibility of the on-chip ICC for quantification of EGFR, PTEN, pAkt and pS6 expression, we performed three independent MIC measurements of U87-PTEN-EGFR cells in normal serum media. *A*, Histograms from the three independent experiments show minimal differences for EGFR, PTEN, pAkt and pS6 expression. For reference, we also plot histograms of the appropriate negative controls, including U87 cells for EGFR and PTEN, erlotinib-treated (20 μM, 2 days) U87-PTEN-EGFR cells for pAkt, and rapamycin-treated (20 nM, 2 days) U87-PTEN-EGFR cells for pS6. *B*, Statistical analysis of reproducibility among replicate measurements of EGFR, PTEN, pAkt and pS6. To confirm that the EGFR, PTEN, pAkt and pS6 histograms were statistically reproducible, we calculated the t-score among replicates. All log-transformed data were approximately normally distributed. For EGFR, PTEN and pS6, we consistently find *p*-values less than 0.3, indicating that the mean value did not vary significantly among the replicates. For pAkt, the *p*-values are occasionally higher (e.g., $p = 0.83$ when comparing replicates #1 vs. #3), but the histograms are still statistically indistinguishable. *C*, Statistical analysis of reproducibility versus negative controls. To confirm that the MIC can reproducibly measure the difference between positive and negative controls, we also calculated the t-score for the replicates against the appropriate negative controls. The *p*-values of all pairs of histograms were less than 0.02 for EGFR & pS6, 0.18 for PTEN and 0.40 for pAkt, suggesting that the MIC can reproducibly measure the difference between positive and negative controls.

Supplementary Fig. S6. Analysis of minimal cell number required for protein detection by Western blotting

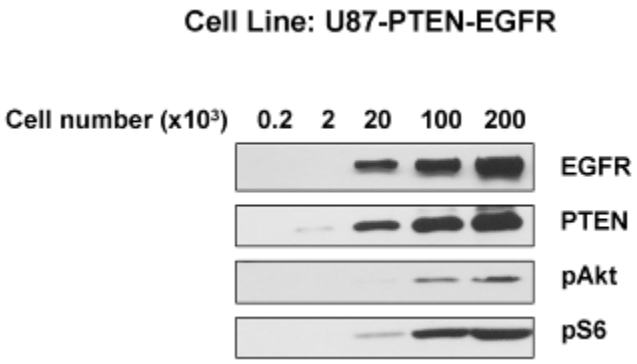

U87-PTEN-EGFR cell lysate was prepared at a concentration of $8x10^7$ cells/mL, and diluted lysates corresponding to $2x10^5$, $1x10^5$, $2x10^4$, $2x10^3$ and 200 cells were analyzed by traditional Western blotting for EGFR, PTEN, pAkt and pS6. Western blotting required at least $2x10^4$ cells to detect PTEN, EGFR, pAkt and pS6 protein expression in U87-PTEN-EGFR cells.

Supplementary Fig. S7. MIC measurements can detect differences in endogenous PTEN expression.

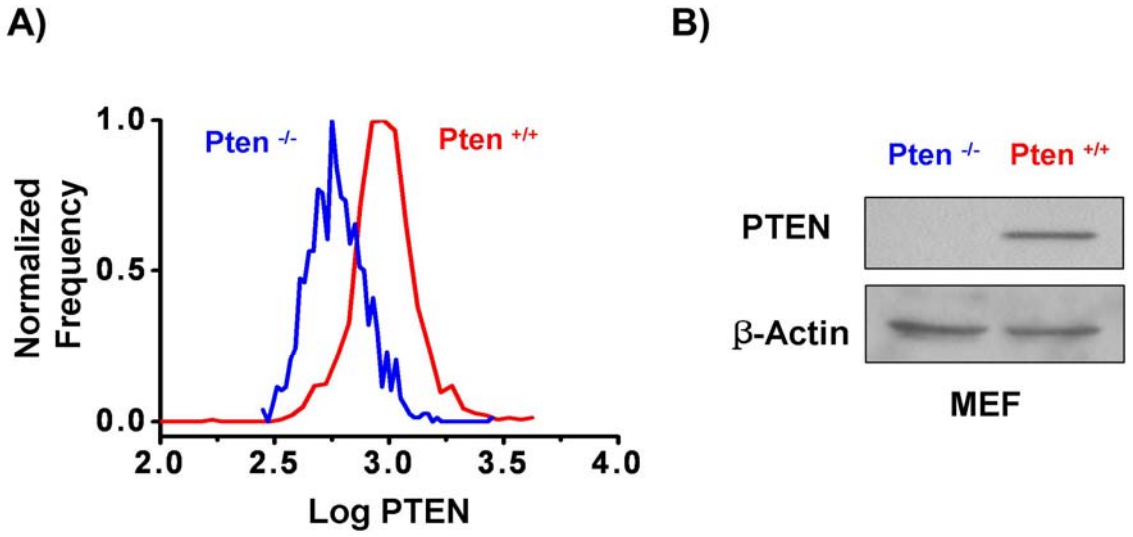

Murine embryonic fibroblast (MEF) PTEN isogenic cell lines (*Pten*$^{-/-}$ and *Pten*$^{+/+}$) (8) were cultured in the cell array chip, and the endogenous PTEN levels were analyzed using the MIC technology. The ICC conditions were similar to those reported in the main text except (i) only PE-conjugated anti-PTEN was used to stain the cells and (ii) the exposure time required for micrograph acquisition was 0.5 sec. *A*, Histograms in MEF *Pten*$^{-/-}$ (blue) and MEF *Pten*$^{+/+}$ (red) revealed quantitative differences in PTEN expression, confirming the MIC technology is sensitive enough to detect difference in endogenous PTEN expression. *B*, Western blotting confirmed MIC-derived results from *A*.

Supplementary Fig. S8. MIC analysis of cellular heterogeneity using individually-stained cell lines.

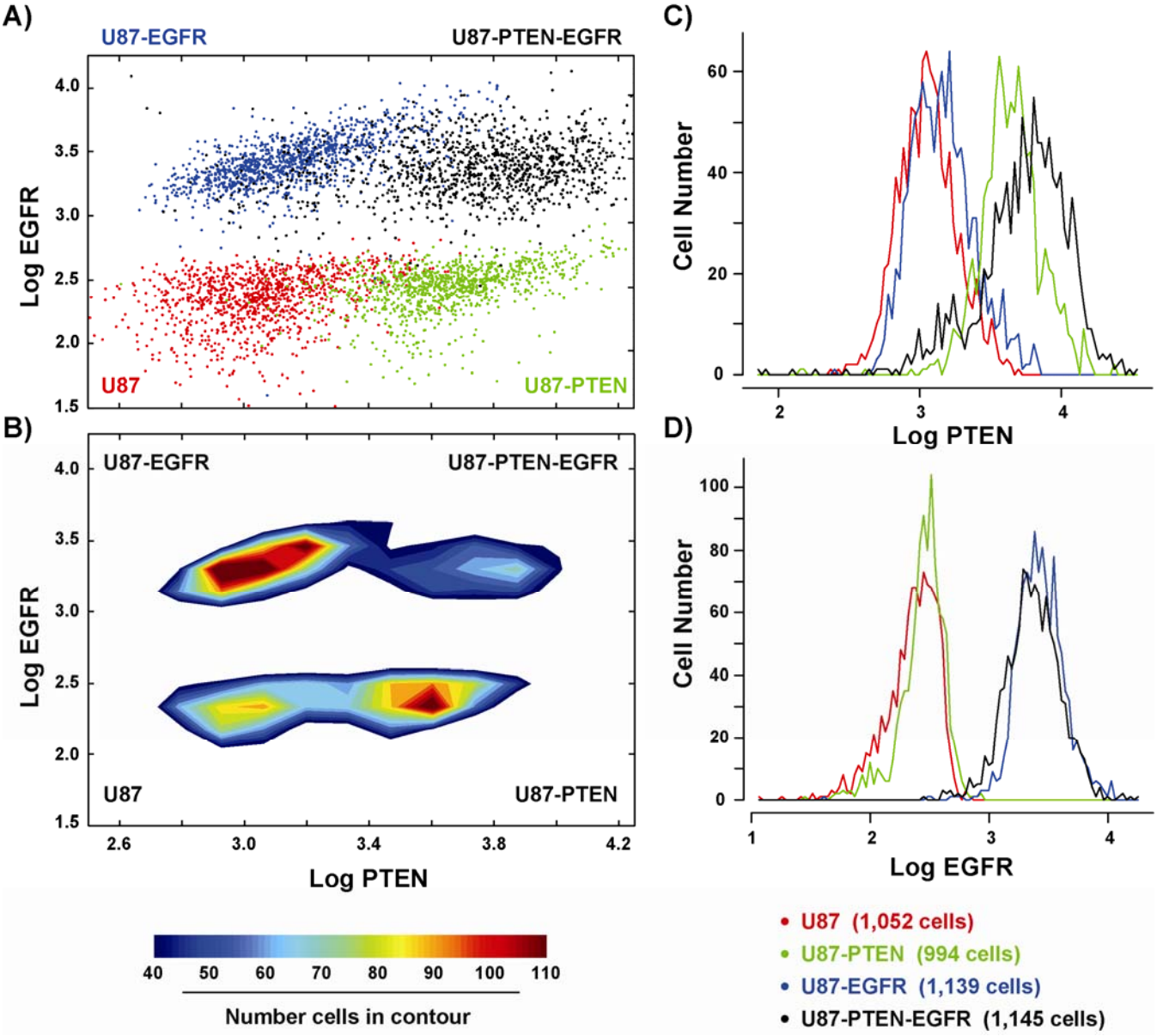

For comparison to analysis of a heterogeneous cell mixture using the MIC platform (Fig. 2*B*-*C*), four U87 cell lines expressing EGFR and/or PTEN (U87, U87-EGFR, U87-PTEN and U87-PTEN-EGFR) (7) were stained individually and the data was mixed *in silico*. *A,* 2D scatter plot of the single-cell PTEN and EGFR measurements for the four U87 cell lines demonstrates the presence of four expected clusters. Note that PTEN expression demonstrates some overlap between high- and low-expressing cells (e.g., U87 and U87-PTEN). *B*, Contour plot of the data in *A*. MIC measurements of the U87 cell mixture (4,330 cells) were plotted on a 2D

contour plot, where color represents the number of cells present in each contour level. The contour plot both confirms the presence of four distinct clusters and corroborates the analysis of cellular heterogeneity in Figure 2*B-C*. Note that the U87-EGFR and U87-EGFR-PTEN cells appear over- and underrepresented in the cell mixture, even though they represent 26.3 and 26.4%, respectively, of the total cell mixture (1,139 and 1,145, respectively, of 4,330 total cells). C and *D*, PTEN and EGFR expression histograms. The separation between high- and low-expressing cell lines is sharper for EGFR than for PTEN, which corresponds to the large separation in EGFR signal observed on the scatter and contour plots. On the PTEN expression histogram, the relatively small separation between U87-EGFR and U87-EGFR-PTEN contributes to the apparent over- and underrepresentation of U87-EGFR and U87-EGFR-PTEN cells on the contour plot.

Supplementary Figure S9. MIC measurements of EGFR, pAkt and pS6 exhibit highly heterogeneous expression profiles in human brain tumor specimens.

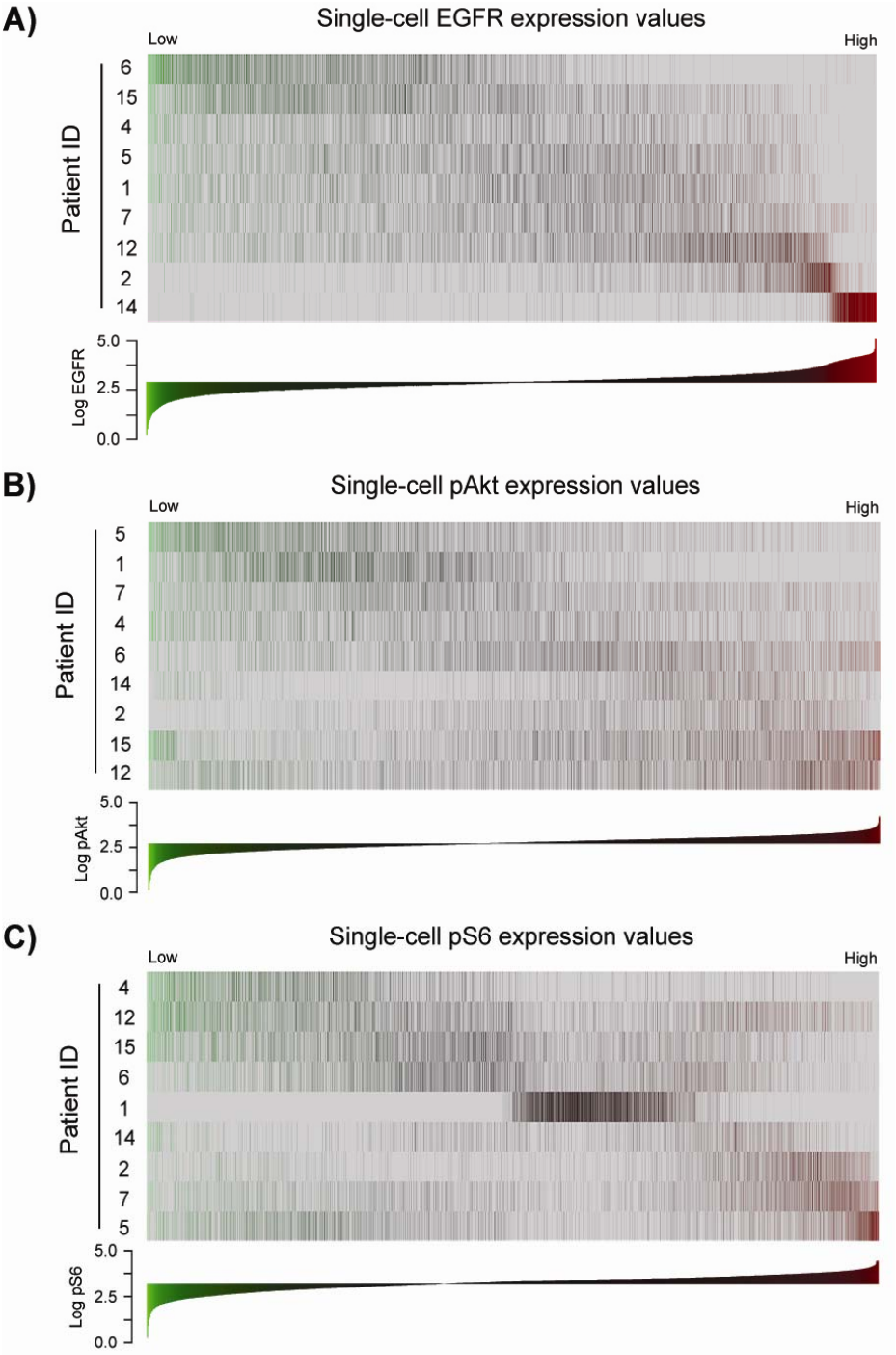

Human brain tumor cells were stained for EGFR, PTEN, pAkt and pS6 using the MIC technology. Single-cell expression data for the same nine patients shown in Figure 3 were sorted from low to high for *A*, EGFR, *B*,

pAkt and *C*, pS6 and plotted on a ranked graph (Supplementary Methods). Each row corresponds to one tumor specimen, and each vertical bar represents one cell from that tumor specimen. To visually represent the intensity of protein expression, vertical bars are colored green and red to indicate low and high protein expression, respectively, as shown on the scale below the rank-based graphs.

Supplementary Fig. S10. Multiple representations of the SOM grid characteristics.

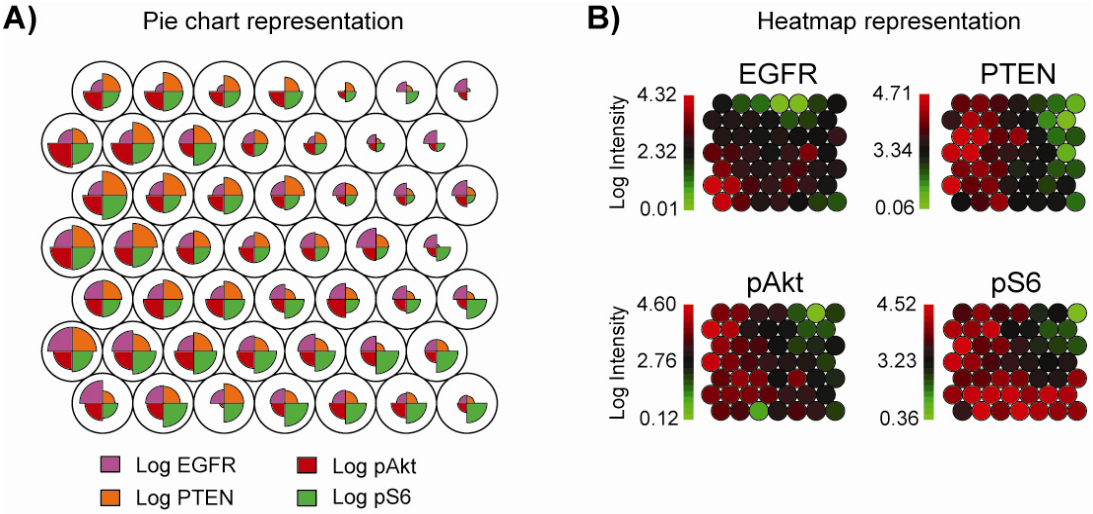

C)

SOM unit	Log EGFR	Log PTEN	Log pAkt	Log pS6	SOM unit	Log EGFR	Log PTEN	Log pAkt	Log pS6
(1,1)	1.69	3.89	3.72	2.96	(5,1)	3.53	4.12	3.22	3.17
(1,2)	0.61	4.13	3.62	3.59	(5,2)	2.74	4.17	3.93	3.27
(1,3)	0.32	3.56	2.65	2.85	(5,3)	2.13	3.95	3.51	3.76
(1,4)	-1.61	3.27	2.86	3.18	(5,4)	2.60	2.57	2.22	3.49
(1,5)	-1.31	2.31	0.79	1.64	(5,5)	2.88	2.79	3.53	2.34
(1,6)	1.10	1.81	-1.08	2.03	(5,6)	2.16	2.19	1.91	2.40
(1,7)	1.94	1.27	1.09	-0.55	(5,7)	2.23	2.04	1.42	3.55
(2,1)	2.28	3.41	5.01	3.82	(6,1)	5.19	5.03	3.58	3.78
(2,2)	2.16	4.49	4.35	3.69	(6,2)	4.19	3.81	3.65	4.28
(2,3)	2.47	3.97	2.41	4.11	(6,3)	2.83	4.05	3.73	4.24
(2,4)	1.61	3.12	2.18	2.11	(6,4)	2.75	3.21	3.29	4.09
(2,5)	0.45	2.69	1.77	1.83	(6,5)	3.24	3.04	2.75	3.67
(2,6)	0.88	1.59	0.77	1.22	(6,6)	2.63	2.24	2.67	4.24
(2,7)	2.02	0.69	0.85	1.15	(6,7)	1.70	2.81	1.83	3.91
(3,1)	2.40	5.04	3.86	4.54	(7,1)	4.77	2.90	3.33	2.63
(3,2)	2.34	4.71	3.20	3.13	(7,2)	3.32	3.73	3.04	4.47
(3,3)	1.59	3.94	2.97	3.39	(7,3)	2.17	4.22	0.02	3.46
(3,4)	2.30	4.21	2.25	2.54	(7,4)	2.47	2.99	2.29	4.34
(3,5)	1.92	2.83	1.14	1.67	(7,5)	2.03	2.86	2.94	3.79
(3,6)	1.79	1.96	1.46	1.24	(7,6)	1.10	2.65	2.67	3.70
(3,7)	2.56	2.20	1.78	1.17	(7,7)	0.62	1.99	1.27	3.61
(4,1)	3.38	4.63	4.41	4.19					
(4,2)	3.12	5.03	3.55	3.66					
(4,3)	2.50	3.68	3.18	2.94					
(4,4)	1.72	3.41	2.80	2.68					
(4,5)	2.54	3.08	2.36	2.34					
(4,6)	3.77	3.00	2.27	2.00					
(4,7)	1.95	1.21	1.33	2.33					

MIC analysis was performed on 19 human brain tumor specimens to quantitate single-cell protein expression levels of EGFR, PTEN, pAkt and pS6. Single-cell 4-parameter data from all tumor specimens were aggregated (~40,000 cells), and a SOM was trained (Supplementary Methods). By testing SOMs of various sizes, we found that a 7x7 SOM was the smallest grid size that reliably showed qualitative differences among the mappings of the 19 tumor specimens (data not shown). *A*, Piechart representation of the 4-parameter vectors characterizing the SOM grid. Each unit of the SOM grid is represented by a vector with characteristic values

for EGFR, PTEN, pAkt and pS6, termed the codebook vector for that unit. To visually represent how these vectors vary over the SOM grid, each unit is divided into quadrants, and the size of the color-coded quadrant represents the intensity of the indicated stain in that unit. *B*, Heatmap representation of the 4-parameter vectors characterizing the SOM grid. To visually the codebook vectors of the SOM grid in a different manner, each stain is depicted in an individual map where red and green represent high and low protein expression, respectively, as shown by the scale bar for each map. *C*, Table describing each SOM unit. The numerical values correspond to the stain intensity as measured from the fluorescent micrographs after background subtraction and $\log_{10}$ transformation. SOM units are numbered as depicted in Figure 4*A*.

Supplementary Fig. S11. Quantitative characterization of patient sample heterogeneity.

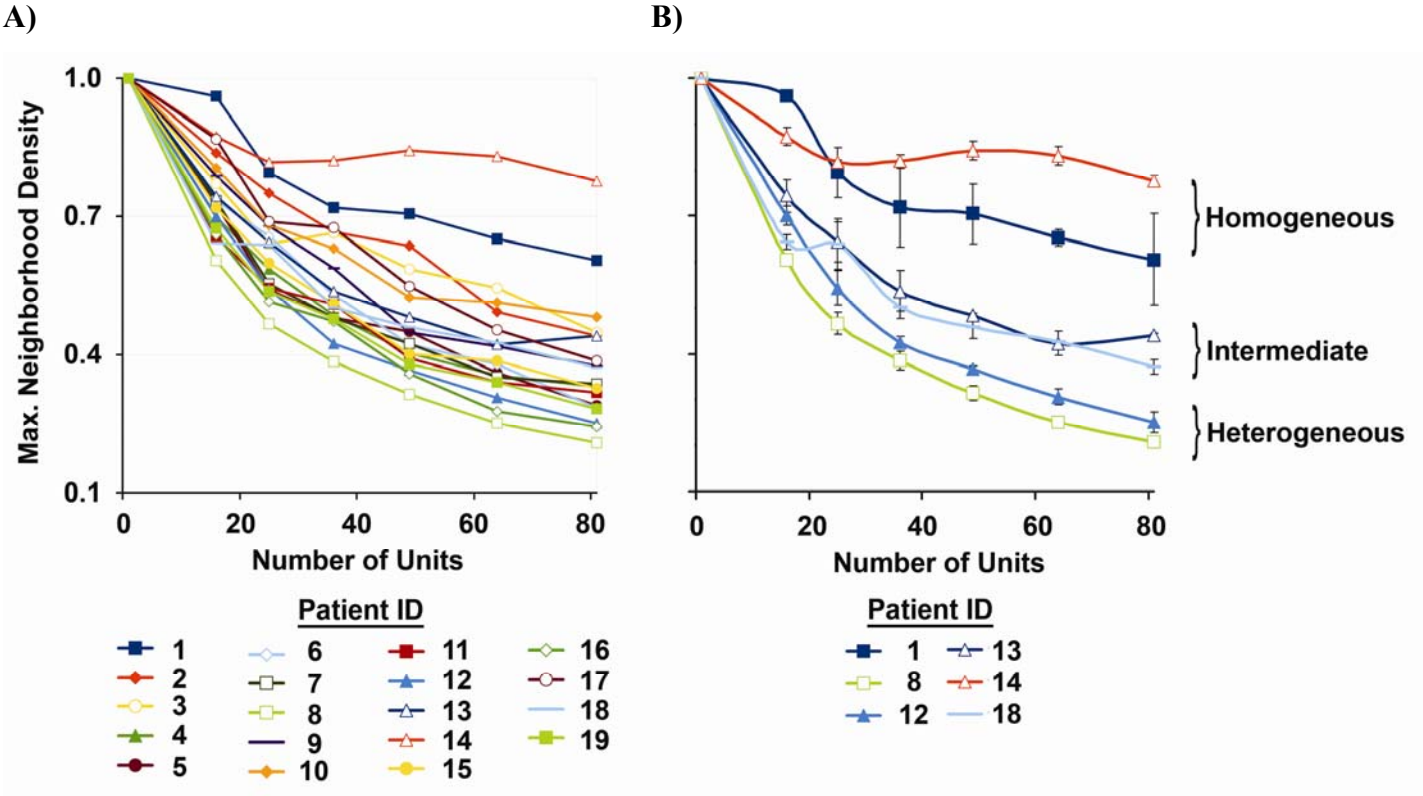

The decay rate of maximum neighborhood density quantitatively measures the heterogeneity of tumor samples. The size of the SOM grid was varied from 16 to 81 grids, and tumor specimens were mapped to various size SOMs. For each grid size, the maximum neighborhood density (the sum of the frequency in a unit and all neighboring units) was calculated and plotted against the number of units. *A*, All measured tumors, and *B*, selected tumors with error bars representing the standard deviation of the neighborhood density from three independently-trained SOMs. For homogeneous tumors (Patients 1 and 14), the maximum neighborhood density exhibits a slow rate of decay, whereas heterogeneous tumors (Patients 8 and 12) show a rapid decay. Tumors of intermediate heterogeneity (Patients 13 and 18) were characterized by two distinctive clusters (Supplementary Fig. S12*C*) and show an intermediate rate of maximum neighborhood density decay.

Supplementary Fig. S12. SOM representation of human tumor specimens.

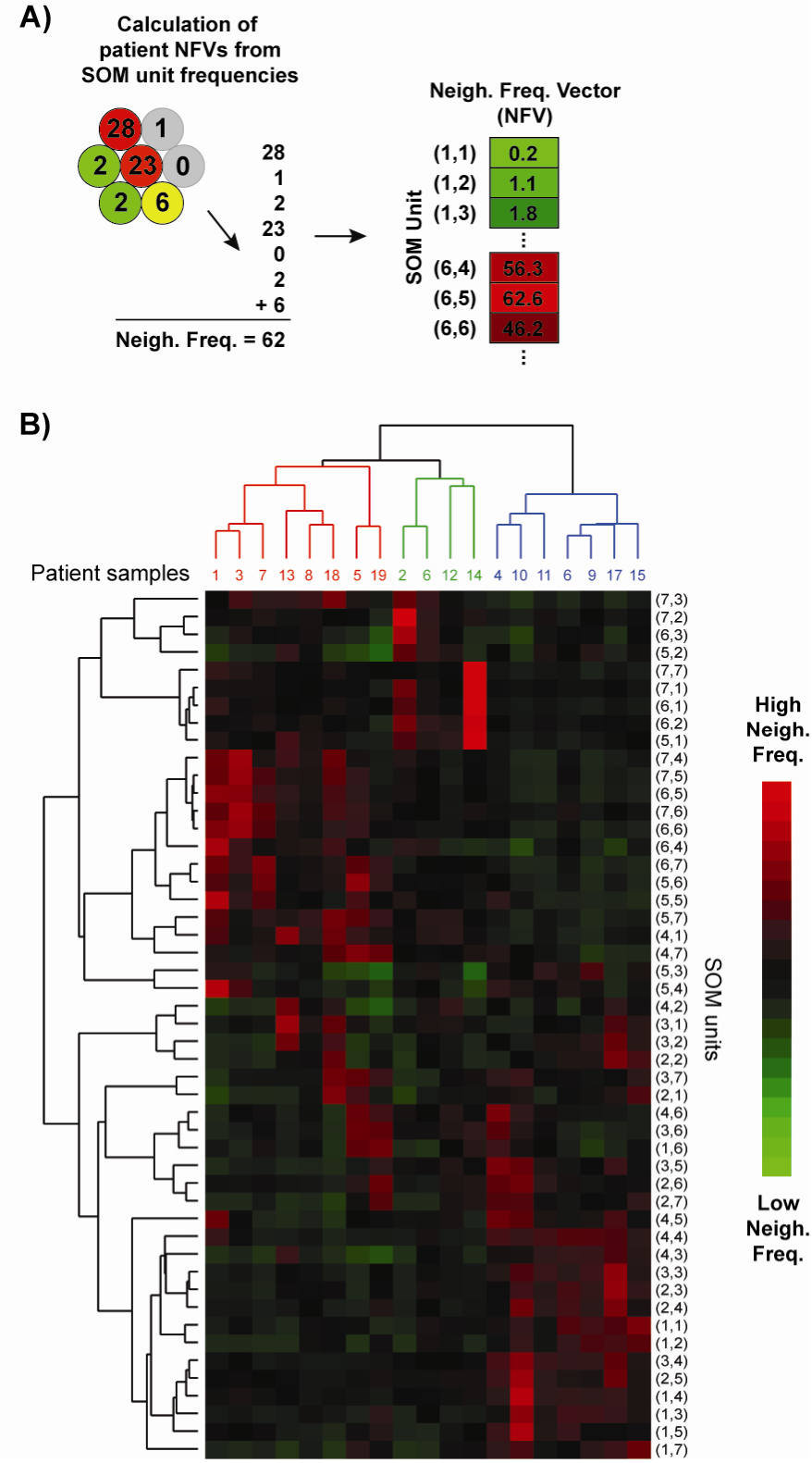

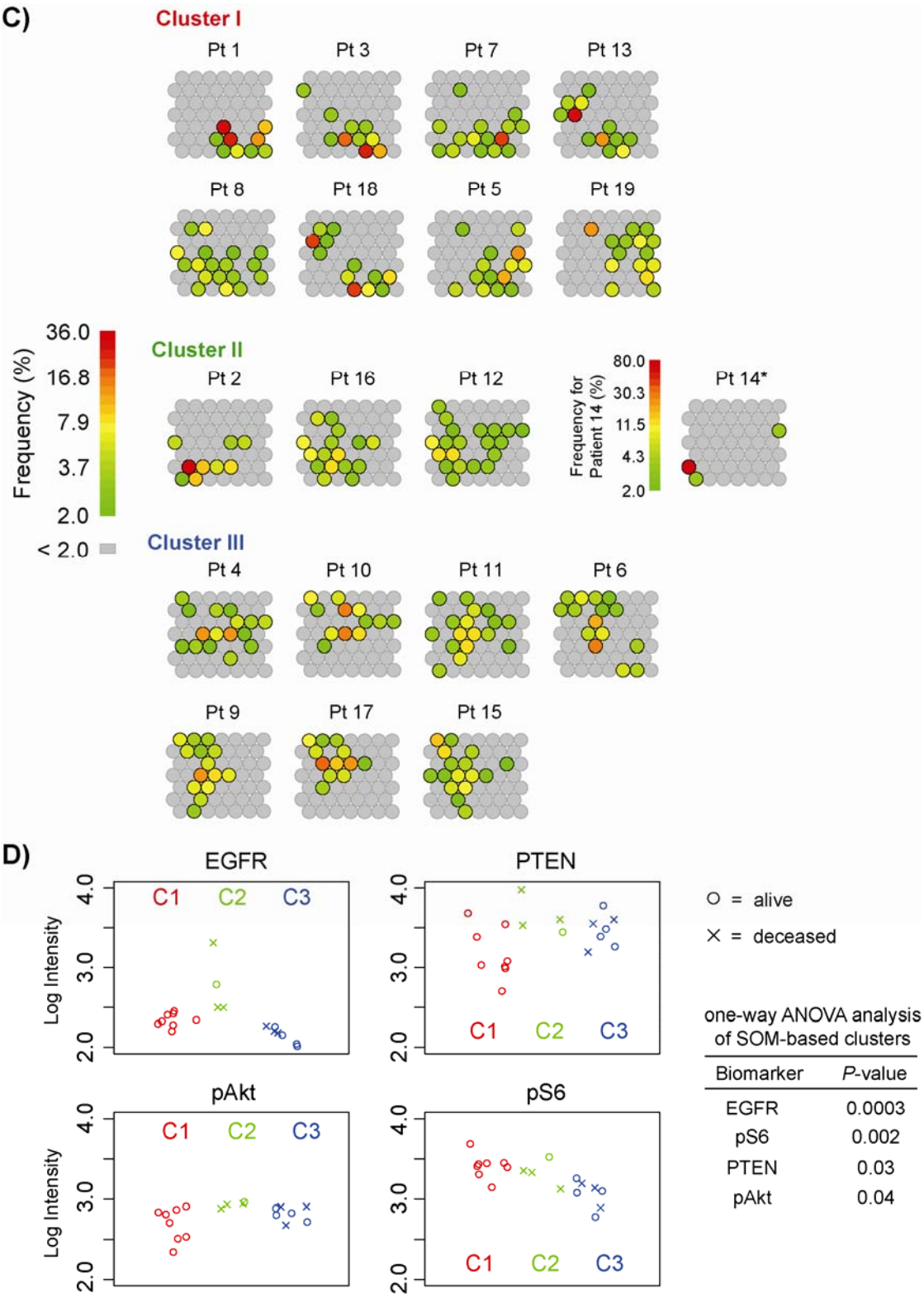

one-way ANOVA analysis of SOM-based clusters

Biomarker	*P*-value
EGFR	0.0003
pS6	0.002
PTEN	0.03
pAkt	0.04

SOM representation and hierarchical clustering of human tumor specimens. *A*, Calcuation of the neighborhood frequency vector (NFV) for hierarchical clustering. For each SOM unit, the neighborhood frequency is the sum

of the frequency of cells mapped to that unit plus the frequencies of all surrounding units as shown. This process is similar to smoothing procedures used in statistics and image processing that capture data patterns while reducing noise. The vector containing these neighborhood frequencies is termed an NFV and is specific to an individual patient sample. *B*, Hierarchical clustering of NFVs for human tumor specimens, including dendrogram for SOM units. For clustering, patient-specific NFVs were subjected to unsupervised hierarchical clustering using the average linkage method based on the Pearson correlation (5). The results were represented using a heatmap where each row corresponds to a SOM unit and each column represents a patient sample. SOM units are numbered according to the diagram shown in Figure 4*A*. Red and green indicate relative high and low neighborhood frequencies, respectively. *C*, SOM projections for all 19 human brain tumor specimens organized by cluster. The single-cell 4 parameter measurements from each tumor specimen were mapped to the SOM grid shown in Supplementary Figure S10, and the frequency of cells that are mapped to each unit was calculated and represented on the $\log_2$ color scales as shown. As denoted by the asterisk, Patient 14 was much more homogeneous than any other measured sample, and thus this sample requires a separate color scale. Qualitative observations based on these SOM projections remained consistent for three independently-trained SOMs. Patient samples were ordered according to the hierarchal clustering. *D*, ANOVA analysis of SOM clusters. The mean EGFR, PTEN, pAkt and pS6 expression for all 19 human brain tumor specimens were segregated by cluster (C1, C2 and C3) and plotted. To determine which of the four biomarkers is most different across the three clusters, ANOVA analysis was used, and *p*-values are shown. Based on the *p*-value, EGFR is the most discriminatory of the four biomarkers between the three clusters, followed in order of decreasing importance by pS6, PTEN and pAkt.

Supplementary Fig. S13. SOM clusters correlate with patient survival and progression.

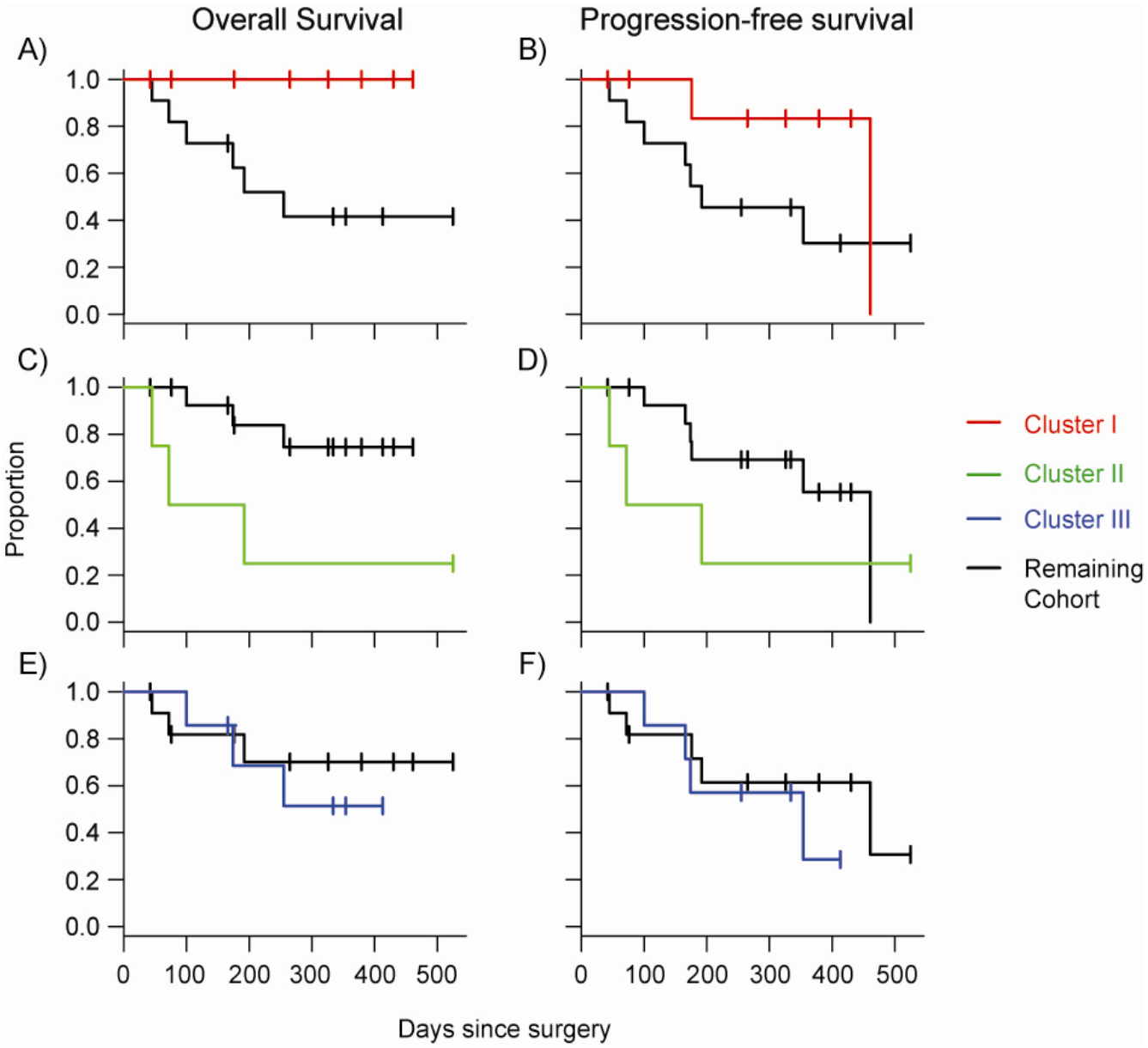

To determine whether the SOM-based clusters (Fig. 4*C* and Supplementary Fig. S12*A*) can predict clinical outcome, we performed survival analysis for each cluster and plotted the results on Kaplan-Meier curves. *A*, *C*, and *E*, Overall survival for clusters I, II, and III, respectively. *B*, *D* and *F*, Progression-free survival for clusters I, II, and III, respectively. Tick marks represent censoring events when patients were lost to follow-up. Cluster I was associated with a significantly lower hazard of death (hazard ratio [HR] < 0.001, $p < 0.001$) whereas Cluster II was associated with a significantly higher hazard of death (HR = 5.4, $p < 0.05$) and Cluster III showed

no significant difference in overall survival compared to the remaining cohort (p = 0.79). Analysis of progression-free survival demonstrated similar trends to overall survival, although none of the hazard ratios were significantly different from the remaining cohort (p = 0.19, 0.33 and 0.523 for Clusters I, II and III, respectively). These data demonstrate the potential of SOM-based clustering of MIC measurements to stratify patients into groups that predict clinical outcome measures.

Supplementary Figure S14. MIC measurements enable dissection of cellular heterogeneity in U87 isogenic cell lines subjected to the tumor dissociation protocol.

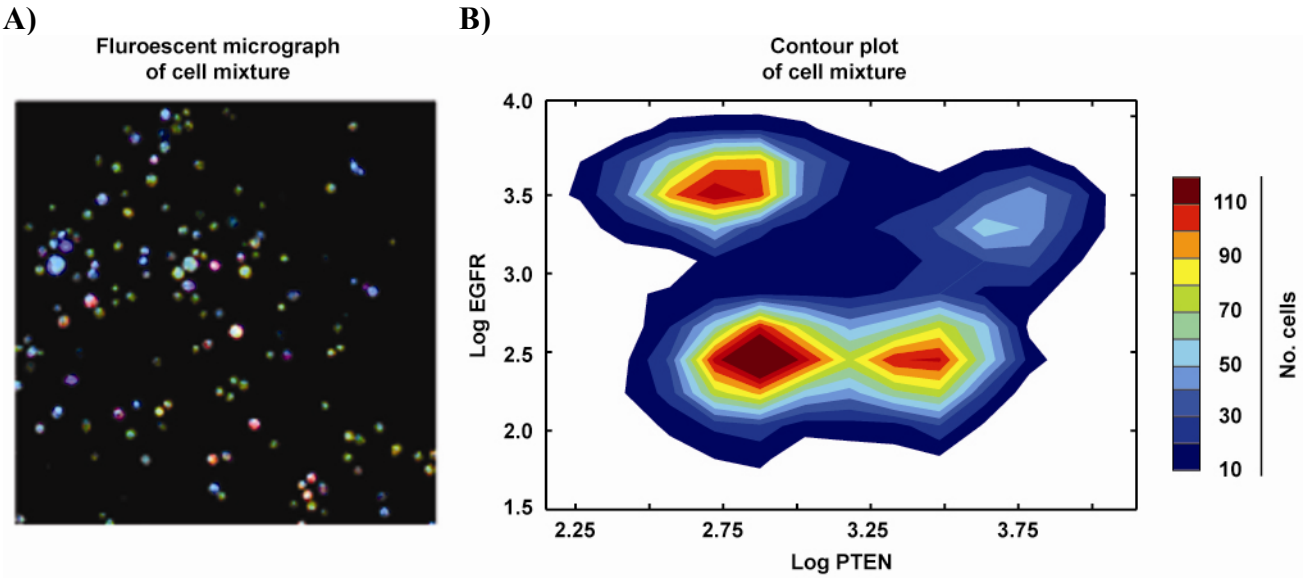

Because dissociated cells from human brain tumor specimens retain a spherical morphology following the tissue processing protocol (Materials and Methods), we verified that this spherical morphology did not affect the capability of MIC analysis to resolve heterogeneous populations of cancer cells by mixing individual U87 isogenic cell lines (U87, U87-EGFR, U87-PTEN and U87-PTEN-EGFR) at an approximately equal ratio, processing the cell mixture using the tumor dissociation protocol and finally subjecting the spherical cells to four-color ICC. Compared to fully-spread U87 cells, the exposure times for micrograph acquisition of spheroid U87 cells were shortened for PTEN (0.02 sec for PE-conjugated anti-PTEN) and pS6 (0.1 sec for Alexa Fluor 488-conjugated anti-pS6) to avoid signal saturation. *A*, A fluorescent micrograph of the cell mixture after staining for EGFR, PTEN, pAkt and pS6. *B*, The 2D contour plot of single-cell EGFR and PTEN expression levels from the U87 cell mixture where color corresponds to the number of cells present in each contour level. This plot both confirms the presence of four clusters and reveals the slight underrepresentation of U87-PTEN-EGFR cells within the cell mixture. These data suggest that i) the MIC technology is capable of dissecting the heterogeneity within mixtures of cells with spherical morphology, and that ii) spherical morphology does not affect the MIC measurement of EGFR and PTEN levels.

REFERENCES

1. Hemmati HD, Nakano I, Lazareff JA, et al. Cancerous stem cells can arise from pediatric brain tumors. Proc Natl Acad Sci U S A 2003; 100: 15178-83.
2. Choe G, Horvath S, Cloughesy TF, et al. Analysis of the phosphatidylinositol 3'-kinase signaling pathway in glioblastoma patients in vivo. Cancer Res 2003; 63: 2742-6.
3. Mellinghoff IK, Wang MY, Vivanco I, et al. Molecular determinants of the response of glioblastomas to EGFR kinase inhibitors. The New England journal of medicine 2005; 353: 2012-24.
4. Wehrens R, Buydens LMC. Self- and super-organizing maps in R: The Kohonen package. J Stat Soft 2007; 21: 1-19.
5. Eisen MB, Spellman PT, Brown PO, Botstein D. Cluster analysis and display of genome-wide expression patterns. Proc Natl Acad Sci U S A 1998; 95: 14863-8.
6. Saldanha AJ. Java Treeview--extensible visualization of microarray data. Bioinformatics 2004; 20: 3246-8.
7. Wang MY, Lu KV, Zhu S, et al. Mammalian Target of Rapamycin Inhibition Promotes Response to Epidermal Growth Factor Receptor Kinase Inhibitors in PTEN-Deficient and PTEN-Intact Glioblastoma Cells. Cancer Res 2006; 66: 7864-9.
8. Freeman DJ, Li AG, Wei G, et al. PTEN tumor suppressor regulates p53 protein levels and activity through phosphatase-dependent and -independent mechanisms. Cancer Cell 2003; 3: 117-30.